

ionizing an impurity band. Since the position of this peak varies with incident intensity, it may indicate heating of the sample at the incident face. At higher fields the series of peaks corresponds to three times the laser photon energy, equaling the valence-band-to-Landau-level separation.³ These three-photon absorption peaks were seen only when the peak of the photoresponse was monitored. For $I_0 \approx 10^5$ W/cm² the saturation region is attained; however, no instability similar to those at LN₂ temperatures was observed at LHe.

III. SUMMARY

These preliminary measurements of properties of multiphoton-injected plasmas indicate several interesting areas for further research. First, it seems possible to inject homogeneous plasmas with densities in the 10^{15} - cm^{-3} range, whose temperatures are very close to the lattice temperature down to at least 10°K . These field-free injected plasmas should be of considerable interest in studying plasmas instabilities in InSb. Some recent results²⁹ indicate interesting interactions between the laser-injected plasma and an electric-field-injected plasma. Shorter CO₂ laser pulses may be able to probe the plasma lifetimes in more detail, using the recombination radiation and constant-voltage photoconduc-

²⁹ R. Slusher, W. Gariat, and B. Ancker-Johnson (unpublished).

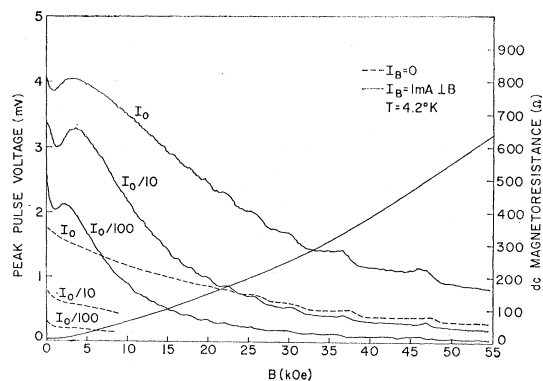


FIG. 7. Magnetic field dependence of peak photoconductive signal during $10.6\text{-}\mu$ laser pulse for $n\text{-InSb}$ at LHe temperature. Other parameters are similar to those in Fig. 6.

tivity as indicators. It is also possible to produce dense ($>10^{14}$ cm^{-3}) plasma in magnetic fields up to 100 kOe using both 9.6- and $10.6\text{-}\mu$ radiation with intensities in the range above 10^5 W/cm².

ACKNOWLEDGMENTS

We would like to thank B. Ancker-Johnson, C. K. N. Patel, and P. A. Wolff for helpful discussions, and J. Strautins for technical assistance.

Calculation of the Reflectivity, Modulated Reflectivity, and Band Structure of GaAs, GaP, ZnSe, and ZnS†

JOHN P. WALTER* AND MARVIN L. COHEN

Department of Physics and Inorganic Materials Research Division, Lawrence Radiation Laboratory, University of California, Berkeley, California 94720

(Received 13 January 1969)

We have calculated the electronic energy band structure, the imaginary part of the frequency-dependent dielectric function, the reflectivity, and the modulated reflectivity (derivative of the reflectivity) for GaAs, GaP, ZnSe, and ZnS, using the empirical pseudopotential method. A direct comparison of the measured and calculated reflectivities is made. The calculated derivative of the reflectivity spectrum is compared with thermoreflectance data.

INTRODUCTION

THE electronic energy-band structure has been calculated by us; also, the imaginary part of the frequency-dependent dielectric function $\epsilon_2(\omega)$; the reflectivity $R(\omega)$; and the modulated reflectivity $R'(\omega)/R(\omega)$, where $R' = dR/d\omega$, for GaAs, GaP, ZnSe, and ZnS, using the empirical pseudopotential method¹

(EPM). In previous calculations² the imaginary part of the frequency-dependent dielectric function $\epsilon_2(\omega)$ was calculated and compared with experiment. However, since the reflectivity is the actual quantity measured, it was felt that a direct comparison between measured and theoretically calculated reflectivity would be desirable. The main reason for wanting a comparison of this type rather than an $\epsilon_2(\omega)$ comparison is that it is necessary to use an integral transform of the reflectivity

† Work supported in part by the National Science Foundation.

* National Science Foundation Graduate Fellow.

¹ M. L. Cohen and T. K. Bergstresser, *Phys. Rev.* **141**, 789 (1966), and references therein.

² W. Saslow, T. K. Bergstresser, C. Y. Fong, M. L. Cohen, and D. Brust, *Solid State Commun.* **5**, 667 (1967).

TABLE I. Comparison of the GaAs, GaP, ZnSe, and ZnS form factors (in Ry) used in the present work (on top) with those used in Ref. 1.

	$V^S(\sqrt{3})$	$V^S(\sqrt{8})$	$V^S(\sqrt{11})$	$V^A(\sqrt{3})$	$V^A(2)$	$V^A(\sqrt{11})$
GaAs	-0.245	-0.005	0.075	0.062	0.035	0.003
	-0.23	0.01	0.06	0.07	0.05	0.01
GaP	-0.225	0.024	0.076	0.128	0.053	0.020
	-0.22	0.03	0.07	0.12	0.07	0.02
ZnSe	-0.223	-0.008	0.068	0.204	0.099	0.022
	-0.23	0.01	0.06	0.18	0.12	0.03
ZnS	-0.249	0.038	0.053	0.195	0.116	0.015
	-0.22	0.03	0.07	0.24	0.14	0.04

tivity over a large energy range to obtain $\epsilon_2(\omega)$, and the experimental reflectivity is usually known only over a limited range of energy.

In the theoretical calculation, $\epsilon_2(\omega)$ is obtained and a Kramers-Kronig analysis is still necessary; however, there are several reasons for believing that the problems in this case are less severe. First, the experimental spectrum may contain exciton effects and this may cause some structure to be weighted in a manner such that a subsequent comparison of theory and experiment is difficult. Second, it is usually possible to calculate the theoretical $\epsilon_2(\omega)$ over a larger energy range than the experimental measurements and to use tail functions to accurately represent the contributions from the higher bands. Finally, surface effects can alter the heights of reflectivity peaks which, in turn, will cause energy shifts in the $\epsilon_2(\omega)$ structure. No such effects are possible in the theory calculations.

Pseudopotential form factors for these crystals were obtained by Cohen and Bergstresser¹ (CB) using the EPM. These form factors were obtained by comparison with the existing optical data.^{1,3-6} New measurements of the optical properties have been made⁷⁻¹³ since that time. The results of these measurements and a direct comparison between the experimental and the theoretical $R(\omega)$ were used to make slight adjustments of the CB form factors.

We have made a critical-point analysis to identify the optical structure in terms of interband transitions. The symmetries and positions in energy of the im-

portant critical points have been determined and their contributions to $\epsilon_2(\omega)$ and $R(\omega)$ have been investigated.

A comparison between theory and experiment shows good agreement for both the reflectivity and the modulated reflectivity. The latter is compared only with thermorefectance data¹¹ and not with other modulated reflectance data, e.g., electroreflectance. The reason for this restriction to thermorefectance is that other methods, such as electroreflectance, involve a more complicated variation of the reflectivity and consequently a simple derivative of the type we have calculated is not appropriate for comparison.

CALCULATIONS

The EPM involves adjusting pseudopotential form factors to achieve good agreement with experimental results for the principal optical transitions. These form factors are then used to determine the electronic energy bands on a fine mesh of points in the Brillouin zone.

The pseudopotential Hamiltonian has the form

$$H = -(\hbar^2/2m)\nabla^2 + V(\mathbf{r}). \quad (1)$$

The weak pseudopotential $V(\mathbf{r})$ is expanded in the reciprocal lattice

$$V(\mathbf{r}) = \sum_{\mathbf{G}} V(|\mathbf{G}|) e^{-i\mathbf{G}\cdot\mathbf{r}}, \quad (2)$$

where \mathbf{G} is a reciprocal-lattice vector. $V(|\mathbf{G}|)$ can be conveniently expressed as

$$V(\mathbf{G}) = V^S(|\mathbf{G}|) \cos\mathbf{G}\cdot\boldsymbol{\tau} + iV^A(|\mathbf{G}|) \sin\mathbf{G}\cdot\boldsymbol{\tau}, \quad (3)$$

TABLE II. Theoretical and experimental reflectivity structure and their identifications, including the location in the Brillouin-zone, energy, and symmetry of the calculated critical points for GaAs. The experimental results are due to Philipp and Ehrenreich.⁸

Reflectivity structure (eV)		Associated critical points		
Theory	Experiment	Location in zone	Symmetry	CP energy (eV)
...	1.48	$\Gamma_{15}-\Gamma_1(0,0,0)$	M_0	1.46
2.95	2.88, 3.15 (spin orbit)	$L_3-L_1(0.5,0.5,0.5)$ $\Delta_3-\Delta_3(0.21,0.21,0.21)$	M_0 M_1	2.69 2.93
4.45	4.55	$\Delta_5-\Delta_1(0.60,0,0)$ (band 4-5)	M_0	4.10
4.85	5.00	$X_3-X_1(1,0,0)$ $\Delta_5-\Delta_1(0.35,0,0)$ (band 4-5)	M_1 M_1	4.34 4.23
5.65	5.55 ^b	$\Sigma_2-\Sigma_1(0.58,0.58,0)$ $\Delta_5-\Delta_1(0.50,0,0)$ (band 4-6)	M_2 M_1	4.76 5.69
6.45	6.6	Volume effect from region around (0.57,0.43,29) (band 4-6) $L_3-L_3(0.5,0.5,0.5)$...	6.35
6.75	6.6	$\Delta_3-\Delta_3(0.43,0.43,0.43)$ (band 3-6 and band 4-7) $\Delta_3-\Delta_3(0.43,0.43,0.43)$ (band 4-6)	M_1 M_3	6.51 6.51

^a Reference 10.

^b This shoulder appears in Greenaway's datum (Ref. 3).

³ D. L. Greenaway, Phys. Rev. Letters **9**, 97 (1962).

⁴ H. R. Philipp and H. Ehrenreich, Phys. Rev. **129**, 1550 (1963).

⁵ M. Aven, T. F. Marple, and B. Segall, J. Appl. Phys. Suppl. **32**, 2261 (1961).

⁶ M. Cardona and G. Harbeke, in *Proceedings of the Seventh International Conference on the Physics of Semiconductors* (Dunod Cie., Paris, 1964), p. 217.

⁷ A. G. Thompson, M. Cardona, K. L. Shaklee, and J. C. Woolley, Phys. Rev. **146**, 601 (1966).

⁸ F. H. Pollak, M. Cardona, and J. Barber (to be published).

⁹ J. W. Baars, in *1967 International Conference on II-VI Semiconducting Compounds*, edited by D. G. Thomas (W. A. Benjamin, Inc., New York, 1967), p. 631.

¹⁰ R. C. Eden, Stanford Electronics Laboratory Technical Report No. 5222-1, 1967 (unpublished).

¹¹ E. Matatagui, A. G. Thompson, and M. Cardona, Phys. Rev. **176**, 950 (1968).

¹² S. S. Vishnubhatla and J. C. Woolley, Can. J. Phys. **46**, 1769 (1968).

¹³ Y. Petroff, M. Balkanski, J. P. Walter, and M. L. Cohen, Solid State Commun. (to be published).

where $\tau = \frac{1}{8}a(1,1,1)$ and a is the lattice constant. In these calculations only the six form factors $V^s(\sqrt{3})$, $V^s(\sqrt{8})$, $V^s(\sqrt{11})$, $V^A(\sqrt{3})$, $V^A(2)$, and $V^A(\sqrt{11})$ are allowed to be nonzero; i.e., zero values are taken for $G^2 \geq 12$ and when the structure factors $\cos \mathbf{G} \cdot \tau$ and $\sin \mathbf{G} \cdot \tau$ are zero.

The solution of (1), using the form factors in (3), allows a calculation of $E(\mathbf{k})$ at many points in the Brillouin zone. This permits us to calculate the imaginary part of the dielectric function using

$$\epsilon_2(\omega) = \frac{e^2 \hbar^2}{3\pi m^2 \omega^2} \sum_{c,v} \int \delta(E_c(\mathbf{k}) - E_v(\mathbf{k}) - \hbar\omega) \times |\langle U_{k,v} | \nabla | U_{k,c} \rangle|^2 d^3k, \quad (4)$$

where $U_{k,v}$ and $U_{k,c}$ are the periodic parts of the valence- and conduction-band wave functions, and the integration is performed over the entire Brillouin zone. The summation is over the highest three valence bands and the lowest six conduction bands. $\epsilon_2(\omega)$ is calculated precisely as described by Saslow *et al.*,² with the one modification that each cube is divided into 512 equal subcubes.

An analytic tail replaces the calculated $\epsilon_2(\omega)$ for higher energies. This is done to account for the high-energy transitions which are not represented in our nine-band $\epsilon_2(\omega)$ calculation. The tail function used is $\beta\omega/(\omega^2 + \gamma^2)^2$, where $\gamma = 4.5$ eV, and β is determined by continuity with $\epsilon_2(\omega)$ at the energy where the transitions neglected in our band cutoff become important. The tail function begins at 8.85 eV for GaAs, 8.95 for GaP, 10.85 for ZnSe, and 10.95 for ZnS. A Kramers-Kronig transformation gives $\epsilon_1(\omega)$; this function

TABLE III. Theoretical and experimental reflectivity structure and their identifications, including the location in the Brillouin zone, energy, and symmetry of the calculated critical points for GaP. The experimental results are due to Philipp and Ehrenreich.^a

Reflectivity structure (eV)		Associated critical points		CP energy (eV)
Theory	Experiment	Location in zone	Symmetry	
...	2.80	$\Gamma_{15}-\Gamma_1(0,0,0)$	M_0	2.79
3.70	3.70	$L_3-L_1(0.5,0.5,0.5)$	M_0	3.40
		$\Lambda_3-\Lambda_1(0.15,0.15,0.15)$	M_1	3.76
4.7	4.6	$\Delta_5-\Delta_1(0.71,0,0)$ (band 4-5)	M_0	4.50
		$X_3-X_1(1,0,0)$	M_1	4.57
5.3	5.3	$\Delta_5-\Delta_1(0.30,0,0)$ (band 4-5)	M_3	4.72
		$\Sigma_2-\Sigma_1(0.50,0.50,0)$	M_2	5.20
6.7	6.9	Volume effect from region around (0.50,0.43,0.29) (band 4-6)	...	6.5
		$L_3-L_3(0.5,0.5,0.5)$	M_2	6.57
6.9	6.9	$\Lambda_3-\Lambda_3(0.37,0.37,0.37)$ (band 3-6 and band 4-7)	M_1	6.68
		$\Lambda_3-\Lambda_3(0.37,0.37,0.37)$ (band 4-6)	M_3	6.68

^a Reference 10.

TABLE IV. Theoretical and experimental reflectivity structure and their identifications, including the location in the Brillouin zone, energy, and symmetry of the calculated critical points for ZnSe. The experimental results are due to Petroff and Balkanski.^a

Reflectivity structure (eV)		Associated critical points		CP energy (eV)
Theory	Experiment	Location in zone	Symmetry	
2.9	2.9	$\Gamma_{15}-\Gamma_1(0,0,0)$	M_0	2.90
4.85	4.75, 5.05	$L_3-L_1(0.5,0.5,0.5)$ (spin orbit)	M_0	4.59
		$\Lambda_3-\Lambda_1(0.31,0.31,0.31)$	M_1	4.73
...	6.00	$X_3-X_1(1,0,0)$	M_0	5.99
6.55	6.63	$\Delta_5-\Delta_1(0.64,0,0)$ (band 4-5)	M_1	6.20
		$\Sigma_2-\Sigma_1(0.64,0.64,0)$ (band 4-5)	M_2	6.63
7.3	7.25	$\Delta_5-\Delta_1(0.41,0,0)$ (band 4-6)	M_0	7.06
		$\Delta_5-\Delta_1(0.57,0,0)$ (band 4-6)	M_1	7.23
7.55	7.6	$\Sigma_1-\Sigma_1(0.20,0,0)$ (band 3-6)	M_1	7.48
...	7.8	$\Gamma_{15}-\Gamma_{15}(0,0,0)$	degenerate	7.84
8.35	8.28, 8.46	Volume effect from region around (0.64,0.43,0.29) (band 4-6)	...	8.25
9.05	8.97, 9.25	$\Lambda_3-\Lambda_3(0.36,0.36,0.36)$ (band 4-7)	M_1	8.79
		$\Lambda_3-\Lambda_3(0.36,0.36,0.36)$ (band 3-6)	M_2	8.79
9.6	9.7	Volume effect from region around (0.43,0.14,0.07) (band 3-7)	...	9.35

^a Reference 13.

together with $\epsilon_2(\omega)$ allows a calculation of the reflectivity $R(\omega)$.

The Cohen and Bergstresser pseudopotential form factors were used as our starting point. By the process described above, we calculated $\epsilon_2(\omega)$ and $R(\omega)$ and then compared $R(\omega)$ with the experimental reflectivity. Much of the gross detail was the same and thus the most important identifications were easily made. By varying the form factors slightly we attempted to move the major peaks to agree more closely to experiment and to duplicate the finer structure. The CB form factors were constrained in the following way: The symmetric form factors for GaAs and ZnSe were made to agree with the Ge-potential, which is in the same row of the Periodic Table; the GaP and ZnS symmetric form factors were set equal to an average of the Group-IV elements corresponding to the rows involved, i.e., an average of Si and Ge. This constraint was relaxed when we made our "fine" adjustment of the form factors. A comparison of the CB form factors and those used in the present calculation are given in Table I. The largest variation is about 0.02 Ry.

In order to shift the reflectivity peaks or shoulders in a predictable manner, we had to determine the transitions responsible for the major contributions to these structures. This was done by finding the energy of the desired peak or shoulder on the $\epsilon_2(\omega)$ graph and then examining the contributions to ϵ_2 at that energy from

TABLE V. Theoretical and experimental reflectivity structure and their identifications, including the location in the Brillouin zone, energy, and symmetry of the calculated critical points for ZnS. Experiment 1 refers to Aven, Marple, and Segall.^a Experiment 2 refers to Baars.^b

Theory	Reflectivity structure (eV)		Associated critical points		
	Experiment 1	Experiment 2	Location in zone	Symmetry	CP energy (eV)
3.8	3.66, 3.76 (spin orbit)	3.68, 3.75 (spin orbit)	$\Gamma_{15}-\Gamma_1(0,0,0)$	M_0	3.74
5.55	5.79	5.78	$L_3-L_1(0.5,0.5,0.5)$ $\Delta_3-\Delta_1(0.32,0.32,0.32)$	M_0 M_1	5.40 5.52
6.6	$X_5-X_1(1,0,0)$	M_0	6.31
7.05	6.99	7.02	$\Delta_5-\Delta_1(0.50,0,0)$ (band 4-5) $\Sigma_2-\Sigma_1(0.53,0.53,0)$	M_1 M_2	6.99 7.08
7.55	7.41	7.5	$\Delta_5-\Delta_1(0.37,0,0)$ (band 4-6) $\Delta_5-\Delta_1(0.51,0,0)$ (band 4-6)	M_0 M_1	7.45 7.57
...	$\Gamma_{15}-\Gamma_{15}$	degenerate	7.79
8.45	...	8.35	Volume effect from region around $(0.57,0.36,0.14)$ (band 4-6)	...	8.35
9.15	...	9.0	$\Delta_3-\Delta_3(0.29,0.29,0.29)$ (band 3-6) Volume effect (bands 3-6 and bands 4-7)	M_1 ...	8.64 8.85
9.75	9.8	9.6	Volume effect (bands 3-6 and bands 4-7)	...	9.5

^a Reference 5.

^b Reference 9.

the constituent interband transitions. When we had determined the interband transition contributing the greatest amount, e.g., bands 4 to 5, we examined a table of energy differences for these bands throughout the Brillouin zone. Particular attention was given to locating critical points with energy in the vicinity of the energy of the optical structure, although volume effects

and the relative size of the momentum matrix elements were also used to determine the probable origin of the structure; the ultimate test of the correctness of our labelling was to change the pseudopotential slightly, to note how the energy splitting changed at that transition point, and finally to see if the peak position changed by the same amount as the energy splitting. All of the prominent reflectivity structure was labelled by this procedure.

To further elucidate this procedure, let us examine the large ϵ_2 peak which occurs at 4.7 eV for GaAs. The value of ϵ_2 at that energy is 31.0. From our tables of interband transitions the major contributions to that peak are bands (4-5), 26.2, bands (3-5), 2.7, bands (4-6), 1.4, with other bands contributing even smaller amounts. Thus transitions from bands (4-5) are almost totally responsible for this peak. An examination of the energy differences between bands 4 and 5 throughout the Brillouin zone reveals that an M_2 critical point occurs along the Σ direction at 4.76 eV with large oscillator strength. Furthermore, we observe that if by varying the form factor slightly the energy splitting at that point is changed by an amount Δ , then the position of the ϵ_2 peak changes by Δ with insignificant error. We therefore conclude that the GaAs peak at 4.7 eV can be labelled by the transition $\Sigma_2-\Sigma_1$.

For the determination of the form factors from the experimental data, six structural features of $R(\omega)$ are chosen as being particularly descriptive of that function. These structures include the basic gap and the major peaks. In order to determine how the form factors

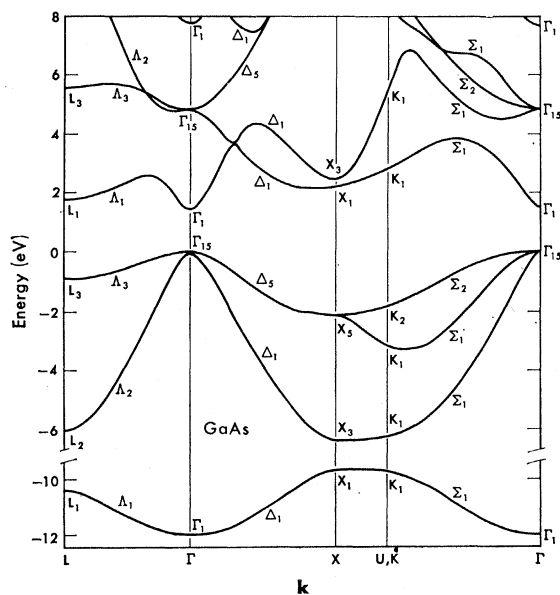


FIG. 1. Band structure of GaAs along the principal symmetry directions.

should be varied, we use the following expression:

$$E_i = E_i^0 - \sum_{j=1}^6 \left(\frac{\partial E_i}{\partial F_j} \right)^0 (F_j - F_j^0), \quad (5)$$

where the F_j^0 are the six nonzero CB form factors and the E_i^0 are the six characteristic energy splittings. $(\partial E_i / \partial F_j)^0$ are the derivatives of the characteristic energy splittings with respect to the form factors, evaluated at the CB form factors. The E_i are the experimental characteristic splittings and the F_j are the new form factors. In practice this equation is useful only in the range $|F_j - F_j^0| \leq 0.01$ Ry. If we define $\Delta E_i \equiv E_i - E_i^0$, $\Delta F_j \equiv F_j - F_j^0$, and $A_{ij} \equiv (\partial E_i / \partial F_j)^0$, then Eq. (5) may be written

$$\Delta E_i = \sum_{j=1}^6 A_{ij} \Delta F_j, \quad \text{only if } |\Delta F_j| \leq 0.01. \quad (6)$$

The terms ΔE_i are known and the terms A_{ij} can be easily calculated. This equation cannot be merely inverted because the ΔE_i are sufficiently large for some j that $|\Delta F_j| > 0.01$, and consequently Eq. (6) no longer correctly describes the situation. We therefore use a gradient projection method of nonlinear programming.¹⁴ The function

$$P = \sum_{i=1}^6 (\Delta E_i - \sum_{j=1}^6 A_{ij} \Delta F_j)^2$$

is a measure of the goodness of the fit to the experimental points. P is minimized subject to the constraints $|\Delta F_j| \leq 0.01$. P must decrease if the matrix A is nonzero, but if P is still too large after this process is completed, the new form factors replace the old and the process is repeated. We have found it necessary to perform at least two iterations before satisfactory agreement is achieved between theory and experiment at the characteristic points. This procedure does not guarantee that P can be made equal to zero but after each iteration P can be no larger than the previous P . We note, however, that the final form factors do not necessarily constitute a unique solution to the problem.

For GaAs, the following six splittings and identifications are used to characterize $R(\omega)$: $\Gamma_{15}-\Gamma_1$ (1.54 eV), L_3-L_1 (2.68 eV), $\Sigma_2-\Sigma_1$ (4.75 eV), $\Delta_5-\Delta_1$ (4-6) (5.55 eV), volume effect (4-6) (6.35 eV), and L_3-L_3 (6.40 eV). For GaP, $\Gamma_{15}-\Gamma_1$ (2.80 eV), L_3-L_1 (3.45 eV), $\Sigma_2-\Sigma_1$ (5.12 eV), volume effect (4-6) (6.52 eV), L_3-L_3 (6.60 eV), and $\Lambda_3-\Lambda_3$ (6.60 eV). For ZnSe, $\Gamma_{15}-\Gamma_1$ (2.90 eV), L_3-L_1 (4.75 eV), $\Sigma_2-\Sigma_1$ (6.75 eV), $\Delta_5-\Delta_1$ (4-6) (7.00 eV), volume effect (4-6) (8.25 eV), and $\Lambda_3-\Lambda_3$ (8.75 eV). For ZnS, $\Gamma_{15}-\Gamma_1$ (3.72 eV), L_3-L_1 (5.55 eV), $\Sigma_2-\Sigma_1$ (7.00 eV), $\Delta_5-\Delta_1$ (4-6) (7.35 eV), volume effect (4-6) (8.35 eV), and $\Lambda_3-\Lambda_3$ (8.75 eV).

¹⁴ J. B. Rosen, *J. Soc. Indust. Appl. Math.* 8, 181 (1960).

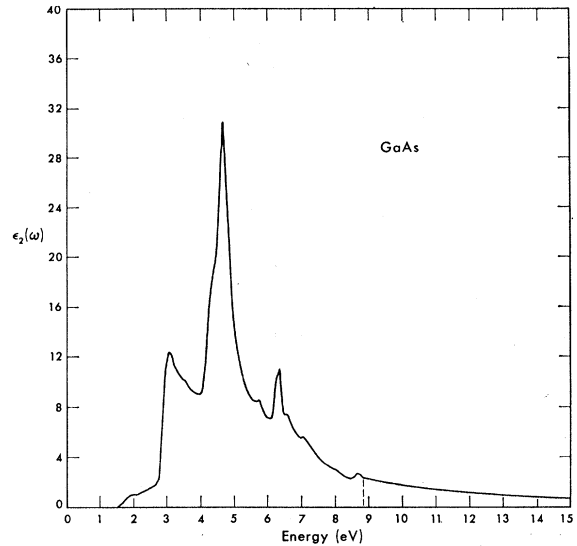


FIG. 2. Theoretical $\epsilon_2(\omega)$ for GaAs. The tail function begins at 8.85 eV.

RESULTS

The band structures in the principal symmetry directions and graphs of selected optical functions are shown in Figs. 1-15. Table I presents a comparison of the CB form factors and those derived in this work. Tables II-V tabulate the important critical points for the four compounds.

GaAs

The threshold in $\epsilon_2(\omega)$ at 1.46 eV is caused by $\Gamma_{15}-\Gamma_1$ transitions (Figs. 1-4). The rise and peak in the 2.7-3.1-eV region corresponds to L_3-L_1 transitions at 2.69 eV and $\Lambda_3-\Lambda_1$ transitions at 2.93 eV. The prominent peak at 4.7 eV is caused almost entirely by $\Sigma_2-\Sigma_1$ transitions in the vicinity of (0.58, 0.58, 0) (units of $2\pi/a$). Some contribution comes from the shoulder on the left

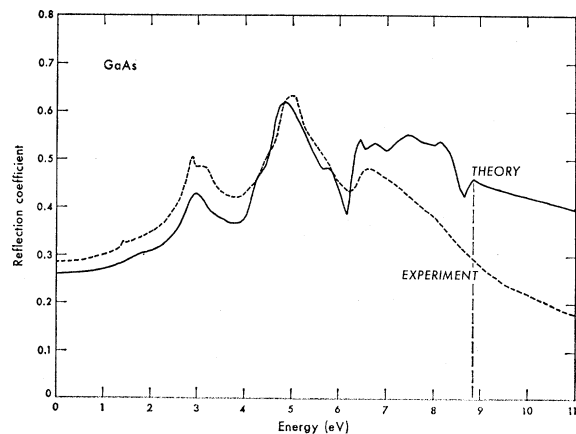


FIG. 3. Comparison of theoretical and experimental $R(\omega)$ for GaAs. The experimental results are due to Philipp and Ehrenreich and appear in Ref. 10. The tail function begins at 8.85 eV for $\epsilon_2(\omega)$.

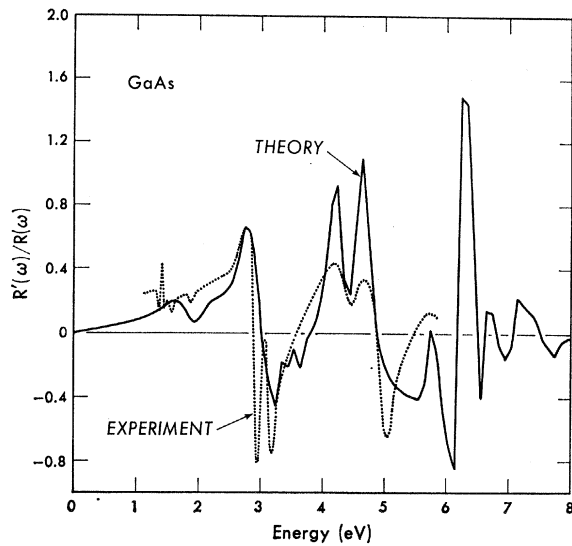


FIG. 4. Comparison for GaAs of theoretical $R'(\omega)/R(\omega)$ with thermoreflectance measurements by Matatagai *et al.* (Ref. 11). The experimental results have been scaled by a constant factor.

side of the peak; this shoulder is attributed to transitions $\Delta_5-\Delta_1$ (M_0 singularity) at 4.10 eV, $\Delta_5-\Delta_1$ (M_1) at 4.23 eV, and X_5-X_1 (M_1) at 4.34 eV. The (4-6) transitions are insignificant in their contribution relative to (4-5) transitions in the vicinity of this peak. The X_5-X_3 transitions at 4.59 eV and $\Gamma_{15}-\Gamma_{15}$ transitions at 4.82 eV create no discernible structure. Changing the energy splittings for these transitions causes no noticeable change in the peak structure. The small peak at 5.7 eV is attributed to $\Delta_5-\Delta_1$ (4-6) transitions at 5.69 eV. The last major peak at 6.35 eV is caused almost entirely by (4-6) transitions within the Brillouin

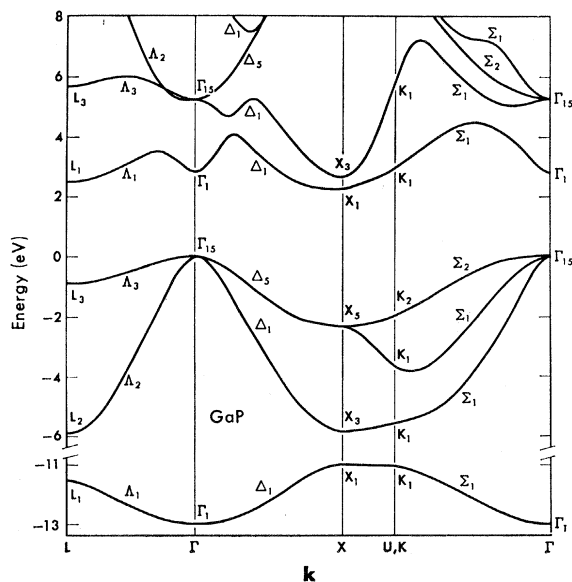


FIG. 5. Band structure of GaP along the principal symmetry directions.

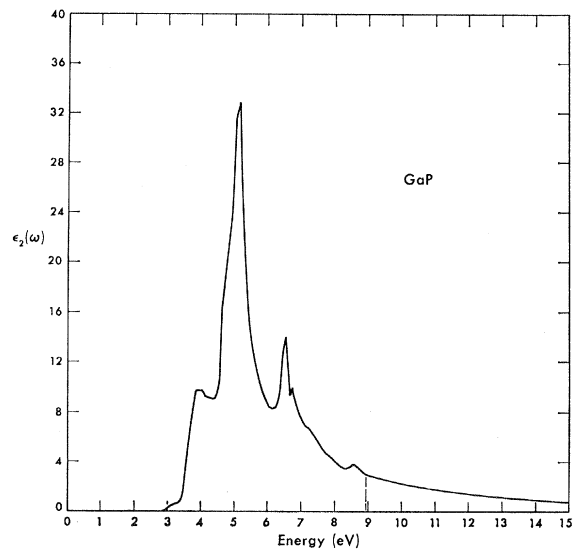


FIG. 6. Theoretical $\epsilon_2(\omega)$ for GaP. The tail function begins at 8.95 eV.

zone in the vicinity (0.57, 0.43, 0.29). Some contribution does come from L_3-L_3 transitions at 6.45 eV, but most of the contribution is from the volume effect. The shoulder at 6.5 eV is caused by $\Lambda_3-\Lambda_3$ transitions, and the last shoulder arises from a volume effect caused by (4-7) transitions.

Plots of both theoretical and experimental reflectivity appear in Fig. 3. The first peak after the small structure at threshold corresponds to the Λ peak occurring at 3.1 eV in $\epsilon_2(\omega)$. The shoulder on the main peak in the reflectivity corresponds to the shoulder on the main ϵ_2 peak and in general each piece of structure in the reflectivity plot has its counterpart on the ϵ_2 plot, displaced by at most 0.25 eV. The experimental reflectivity shows a doublet peak at 2.90 and 3.14 eV, which is attributed to spin-orbit splitting. In addition, this peak has greater magnitude than the theoretical peak. This can be attributed to exciton effects,¹⁵⁻¹⁷ which can occur at this band edge for all four compounds under consideration. Our theory does not take into account either spin-orbit splitting or exciton effects. This agreement between theory and experiment in the vicinity of the main peak is excellent. A shoulder appears in both the experimental and theoretical reflectivity at 4.4 eV. Another shoulder in the theoretical reflectivity appears at 5.65 eV. This can be seen in Greenaway's data³ at 5.55 eV and in Vishnubhatla and Woolley's¹² at 5.45 eV. It is not present in the reflectivity observed by Phillip and Ehrenreich.⁴ Beyond 6.0 eV the experimental reflectivity no longer shows the detailed structure which appears in the theoretical reflectivity.

¹⁵ C. Y. Fong, W. Saslow, and M. L. Cohen, *Phys. Rev.* **168**, 992 (1968).

¹⁶ J. C. Phillips, in *Solid State Physics*, edited by F. Seitz and D. Turnbull (Academic Press Inc., New York, 1965), Vol. 16.

¹⁷ K. L. Shaklee, J. E. Rowe, and M. Cardona, *Phys. Rev.* **174**, 828 (1968).

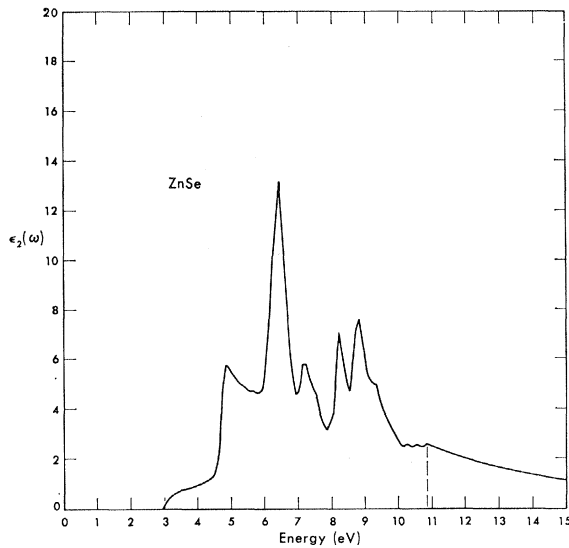


FIG. 10. Theoretical $\epsilon_2(\omega)$ for ZnSe. The tail function begins at 10.85 eV.

4.9-eV region corresponds to L_3-L_1 transitions at 4.59 eV and $\Lambda_3-\Lambda_1$ transitions at 4.73 eV. The prominent peak at 6.45 eV is caused by $\Delta_5-\Delta_1$ (M_1) transitions in the vicinity of (0.64, 0, 0) at 6.20 eV and $\Sigma_2-\Sigma_1$ (M_2) transitions in the vicinity of (0.64, 0.64, 0) at 6.63 eV. X_5-X_1 transitions at 5.99 eV contribute only slightly to the peak. The small peak at 7.2 eV is caused by (4-6) transitions in the Δ direction at 7.06 eV (M_0) and 7.23 eV (M_1). The shoulder at 7.55 eV is attributed to (3-6) (M_1) transitions along Σ at 7.48 eV. $\Gamma_{15}-\Gamma_{15}$ transitions occur at 7.84 eV. The peak at 8.25 eV is caused by (4-6) transitions in a volume centered at (0.64, 0.43, 0.29), which is along the KL line near L . The peak at 8.85 eV is caused chiefly by (4-7) and (3-6) transitions in the Λ direction in the vicinity of (0.36, 0.36, 0.36). The shoulder at 9.35 eV is caused

by (3-7) transitions in a volume centered at (0.43, 0.14, 0.07).

The theoretical and experimental reflectivity appear in Fig. 11. The theoretical peak at 4.85 corresponds to the spin-orbit split experimental peak at 4.75 and 5.05 eV. The theoretical peak is of the same magnitude as the experimental peaks, but it is displaced from the center of the two experimental peaks by 0.05 eV. The next experimental peak occurs at 6.63 eV and has the same shape and roughly the same magnitude as the theoretical peak at 6.65 eV. The experimental reflectivity shows a small peak at 6.0 eV which does not appear in the theoretical reflectivity. However, the X_5-X_1 critical point at 5.99 eV could explain it, since spin-orbit splittings would slightly flatten the bands at X . The theoretical shoulder at 7.3 eV corresponds to the shoulder at 7.25 eV in the experimental data. The steeper slope of the low-temperature data on the right side of the main peak indicates that a low-temperature study in the region of 6.9-7.2 eV might reveal a dip similar to that appearing in the theoretical reflectivity. Another experimental shoulder appears at 7.6 eV, corresponding to a slight shoulder at 7.55 eV for the theoretical reflectivity.

The small peak in the experimental data at 7.8 eV is attributed to $\Gamma_{15}-\Gamma_{15}$ transitions. Although this peak does not appear in the theoretical reflectivity, we expect that the spin-orbit splitting would flatten the bands near Γ and produce this small peak. Since the theoretical peak at 8.35 eV is caused by transitions near L , we expect the peak to be spin-orbit split in the experimental reflectivity. The experimental data does show two peaks at 8.28 and 8.46 eV. The next theoretical peak at 9.05 eV is caused by Λ transitions; the corresponding experimental peaks are spin-orbit split at 8.97 and 9.25 eV. The somewhat flat theoretical peak at 9.6 eV corresponds to the experimental peak at 9.7 eV.

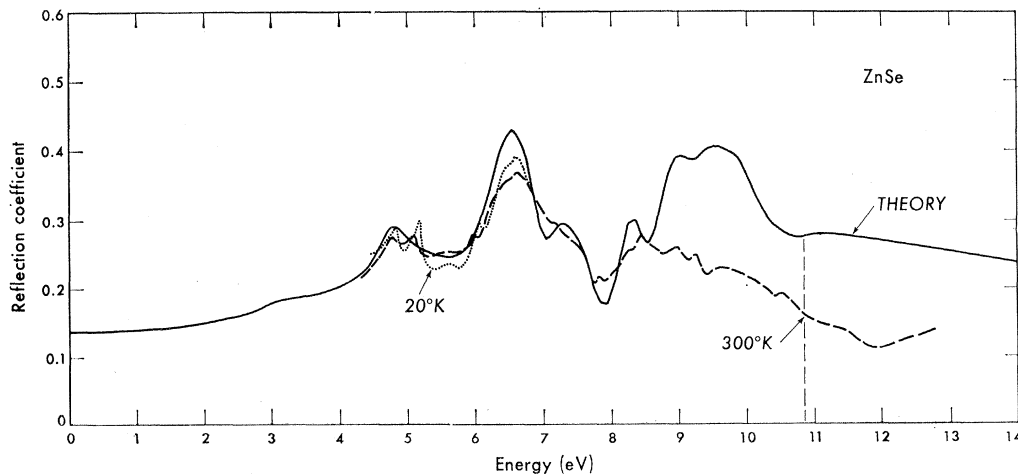


FIG. 11. Comparison of theoretical and experimental $R(\omega)$ for ZnSe. The experimental results are due to Petroff and Balkanski (Ref. 13). The tail function begins at 10.85 eV for $\epsilon_2(\omega)$.

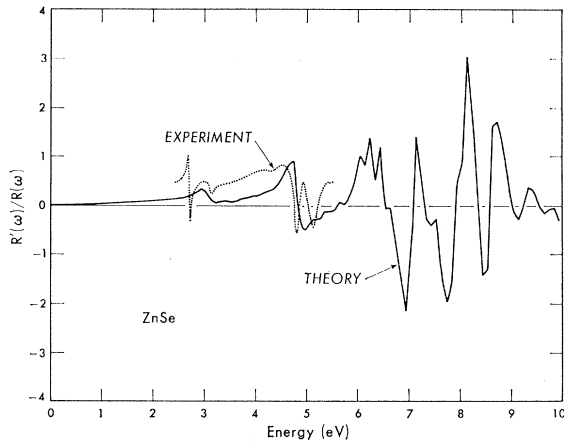


FIG. 12. Comparison for ZnSe of theoretical $R'(\omega)/R(\omega)$ with thermoreflectance measurements by Matatagui *et al.* (Ref. 11). The experimental results have been scaled by a constant factor.

The agreement between experiment and theory is good for ZnSe. In most cases the location of the structure in energy, the shape of the structure, and the height of the structure is the same for theory and experiment.

A comparison of $R'(\omega)/R(\omega)$ and the thermoreflectance appears in Fig. 12.

ZnS

The threshold in $\epsilon_2(\omega)$ is caused by $\Gamma_{15}-\Gamma_1$ transitions at 3.74 eV (Figs. 13–15). The rise and peak in the 5.4–5.7-eV region is caused by L_3-L_1 transitions at 5.40 eV and $\Lambda_3-\Lambda_1$ transitions at 5.52 eV. The principal contributions to the peak at 7.0 eV comes from $\Sigma_2-\Sigma_1$ transitions at 7.08 eV located near (0.54, 0.54, 0) and from $\Delta_5-\Delta_1$ transitions at 6.99 eV located near (0.50, 0, 0). The X_5-X_1 transitions at 6.31 eV also contribute to the peak, causing the slight bulge at 6.5 eV. The small peak at 7.5 eV is caused by (4–6) transitions in the Δ direction at 7.45 and 7.57 eV. The peak subsides with $\Gamma_{15}-\Gamma_{15}$ transitions at 7.79 eV. The peak at 8.35 eV is caused by (4–6) transitions in a volume centered at (0.57, 0.36, 0.14). Although L_3-L_3 transitions also occur at 8.35 eV, changing the energy splitting has negligible effect on the peak, whereas changing the splitting in the vicinity of (0.57, 0.36, 0.14) does change the position of the peak by an amount equal to the change in the splitting. The peak at 8.65 eV is caused principally by (3–6) transitions in the Λ direction. The next two pieces of structure at 8.85 and 9.5 eV are attributed to (3–6) and (4–7) volume transitions.

The data of Cardona and Harbeke⁶ and of Baars⁹ show a small peak at 3.7 eV. The theoretical counterpart is a bump at 3.8 eV. The experimental data shows an exciton-enhanced peak at 5.8 eV. The theoretical peak occurs at 5.6 eV, giving only fair agreement with experiment. The main theoretical peak occurs at 7.05 eV; the measured value is 6.99 eV⁶ and 7.02 eV.⁹

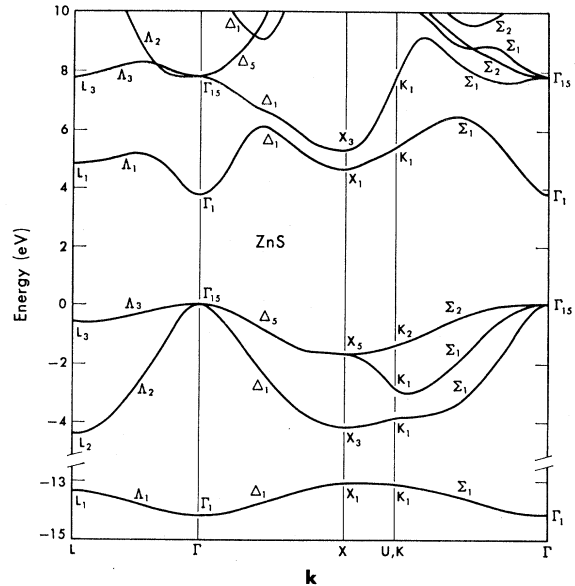


FIG. 13. Band structure for ZnS along the principle symmetry directions.

Shoulders appear in the experimental data at 7.4 and 7.9 eV for Cardona and Harbeke and at 7.5 eV for Baars. The corresponding theoretical shoulder occurs at 7.55 eV. Cardona and Harbeke find a 7.9-eV shoulder which does not appear in the theoretical results or in Baars' data, so it must remain unexplained for the present. Baars' data exhibits peaks at 8.35, 9.0, and 9.6 eV, which are in good agreement with the theoretical peaks at 8.45, 9.15, and 9.75 eV. The data of Cardona and Harbeke has only one peak in this region at 9.8 eV.

We consider the agreement between experiment and theory to be only "fair" compared with the agreement achieved for the other crystals. However, we should

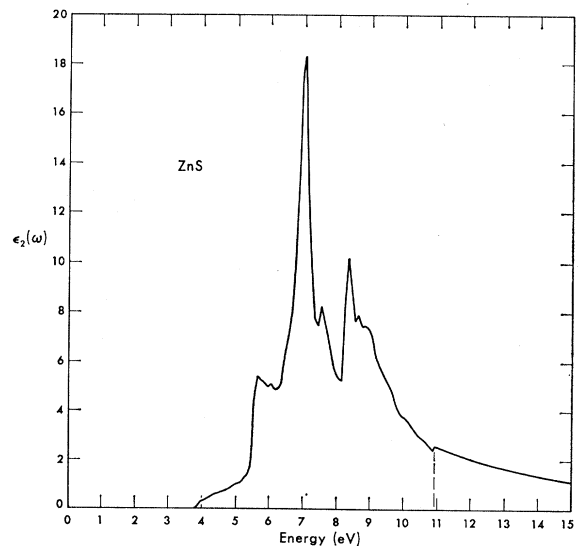


FIG. 14. Theoretical $\epsilon_2(\omega)$ for ZnS. The tail function begins at 10.95 eV.

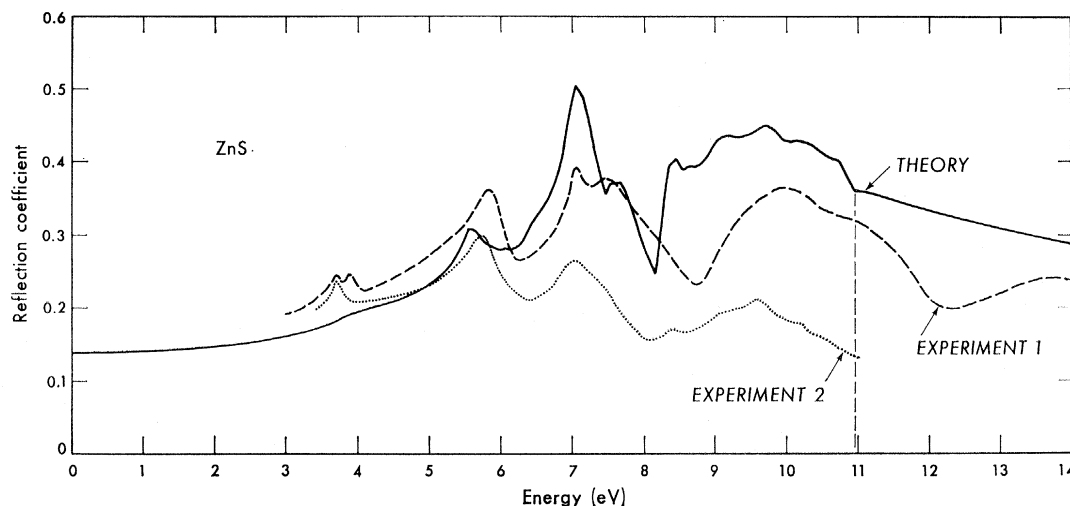


FIG. 15. Comparison of theoretical and experimental $R(\omega)$ for ZnS. Experiment 1 refers to Aven *et al.* (Ref. 5). Experiment 2 refers to Baars (Ref. 9). The tail function begins at 10.95 eV.

point out that there is only fair agreement between the experiments themselves. No thermoreflectance data was available for ZnS; a theoretical curve for $R'(\omega)/R(\omega)$ was therefore, not calculated.

DISCUSSION

We have obtained good agreement between measured and calculated reflectivity and between modulated reflectivity and thermoreflectance. The agreement appears good enough to indicate that our identifications of the important transitions are substantially correct and that our band structure is accurate in the region near the fundamental gap.

The results for GaAs and GaP are good. One point that should be discussed in detail is that in our calculations for GaAs and GaP, the shoulder on the low-energy side of the main Σ peak of $\epsilon_2(\omega)$ is caused by (4-5) transitions along Δ and at X , and that the $\Gamma_{15}-\Gamma_{15}$ transitions do not contribute significantly. A careful study of our band structure reveals that it is consistent with photoemission yield data for GaAs.^{10,18} As the vacuum level¹⁸ is lowered, the first small peak is caused by (4-6) transitions at 4.60 eV along Σ at (0.15, 0.15, 0). The photoemission yield peak becomes larger and shifts its center from 4.65 to 4.50 eV because of (4-6) transitions along Δ (with an average energy of 4.4 eV) and the beginning of massive (4-5) transitions along both Δ and Σ . Eden¹⁰ estimates that $\Gamma_{15}-\Gamma_{15}$ lies in the range of 4.6 to 4.8 eV for GaAs, in good agreement with our value of 4.8 eV, and he estimates a value in the range of 4.8 to 5.2 eV for GaP, as compared with our value of 5.2 eV. If we allow for a small spin-orbit splitting of bands 3 and 4 along the Δ direction, our band structure is also consistent with the electroreflectance measurements of Thompson *et al.*⁷

¹⁸ The experimental data of G. Gobeli and F. Allen appears in M. L. Cohen and J. C. Phillips, *Phys. Rev.* **139**, A912 (1965).

The availability of new and precise data for ZnSe has enabled us to apply the EPM to explore the details in the reflectivity spectrum. The agreement between the calculated and measured reflectivity is very good. We believe the only real differences arise from spin-orbit contributions, and we plan to add spin-orbit terms in the near future to test this conclusion.

For ZnS the fitting procedure was difficult because the experiments differ by a fair amount. In fact, the differences between experiments is greater than that between the theory and either experiment. The agreement is only fair.

For all four crystals the calculated reflectivity at high energies has greater magnitude than the measured reflectivity. Assuming the experimental measurements are accurate in this region, one possibility is that the pseudo-wave-functions might not give accurate oscillator strengths at higher energies. Another possibility is that the high-energy set of calculated ϵ_2 peaks (located at 6-7 eV for GaAs and GaP and at 8-10 eV for ZnSe and ZnS) should be smaller in magnitude and smeared over a slightly larger area, which might occur if we were to include indirect transitions and lifetime effects. [The steep slope followed by the small magnitude of $\epsilon_2(\omega)$ on the high-energy side of these peaks is essentially what causes the high reflectivity.]

A comparison shows that the pseudopotentials for gallium and zinc are in reasonable agreement with the model potentials of Animalu and Heine.¹⁹ The agreement is not precise because our pseudopotential takes into account crystalline effects and is constrained equal to zero for $G^2 > 11$.

ACKNOWLEDGMENT

One of us (J. P. W.) expresses his gratitude to Dr. C. Y. Fong for many helpful discussions.

¹⁹ A. O. E. Animalu and V. Heine, *Phil. Mag.* **12**, 1249 (1965).